ISSN 0020-1685, Inorganic Materials, 2016, Vol. 52, No. 12, pp. 1266–1275. © Pleiades Publishing, Ltd., 2016.
Original Russian Text © T.A. Sedneva, M.L. Belikov, E.P. Lokshin, 2016, published in Neorganicheskie Materialy, 2016, Vol. 52, No. 12, pp. 1343–1352.

Synthesis and Photocatalytic Properties of Nanomaterials Based on Titanium(IV) and Zinc(II) Oxides

T. A. Sedneva*, M. L. Belikov, and E. P. Lokshin

Tananaev Institute of Chemistry and Technology of Rare Elements and Minerals, Kola Scientific Center, Russian Academy of Sciences, Akademgorodok 26a, Apatity, Murmansk oblast, 184209 Russia

**e-mail: sedneva@chemy.kolasc.net.ru*

Received October 22, 2015; in final form, March 28, 2016

Abstract—We have synthesized materials based on titanium(IV) and zinc(II) oxides, containing 1 to 60 wt % Zn, at heat-treatment temperatures from 80 to 1150°C, with the formation of multiphase compositions (X-ray amorphous phase, anatase, rutile, $ZnTiO_3$, and/or Zn_2TiO_4) and studied their phase transitions, morphology, and photocatalytic activity. Increasing the Zn content of the materials is favorable for their spectral sensitization, including the range $\lambda \geq 670$ nm.

Keywords: titanium dioxide, zinc, modification, hydrolysis, photocatalytic activity, spectral range

DOI: 10.1134/S0020168516120098

INTRODUCTION

The need for more efficient solar power conversion in photocatalytic processes for decomposing organic contaminants in the presence of TiO_2, a well-known photocatalyst, requires improving its photocatalytic activity (PCA) in the visible range ($\lambda > 400$ nm) by creating titania-based oxide materials with a band gap under 3.0–3.2 eV. Commercially available TiO_2, supplied by the leading manufacturers Sachtleben, Kemira Pigments Oy, DuPont, Degussa, and others, fails to meet these requirements.

A promising approach for extending the spectral range of TiO_2 PCA to the visible spectral region is doping with various metal ions, which is capable of improving the photocatalytic properties of titania owing to photoinduced carrier separation in doped materials [1–3]. The extension of the spectral range of TiO_2 PCA to the visible and infrared spectral regions by doping with the aliovalent cations W^{6+} and Nb^{5+} was the subject of previous studies [4, 5]. It is of interest to incorporate Zn^{2+} into the crystal structure of titania, because the effect of this ion on the exciton lifetime, charge recombination suppression, and the improved photoelectric and photochemical performance of nanostructured systems considered in previous work [6–12] might be expected to create necessary conditions for a redshift.

In the last decade, there has also been great interest in functional materials design. It has been shown that control over the architecture of TiO_2 at the nanoscale can ensure significant improvements in its functional properties. Crucial for raising the yield of photocatalytic reaction products is the ability to separate oxidizing and reducing centers on the surface of a catalyst by producing layered systems [10], in which photocatalytic reactions may occur both on their surface and in intralayer spaces, so that such materials exhibit sufficiently high PCA. One example is a composite oxide material based on Ti^{4+} and Zn^{2+}, prepared in KOH or NaOH [7, 9] using a number of reagents and containing sodium or potassium titanate nanorods. In addition, in a number of publications the optimal Zn content of aerogels was reported to be 0.5 to 20 wt %.

In this study, alkaline cohydrolysis of Ti and Zn salts in aqueous ammonia is assumed to be a simpler and more effective approach.

The objectives of this work were to study the physicochemical and photocatalytic properties of Ti–O–Zn materials and to assess the feasibility of using them as highly efficient photocatalysts.

EXPERIMENTAL

Samples for this investigation were prepared through the cohydrolysis of the $TiCl_4$ and $ZnCl_2$ salts in aqueous ammonia. First, $ZnCl_2$ was added to a HCl-stabilized $TiCl_4$ solution. Next, the solution was slowly added to 10–12 wt % NH_4OH, as in previous studies [4, 5]. We used reagent-grade chemicals and distilled water. Zinc content was varied from 0.5 to 60 wt %. The resultant samples were heat-treated isothermally in air for 1 h at temperatures from 80 to 1150°C.

The synthesis products were characterized by low-temperature nitrogen adsorption measurements (BET analysis, FlowSorb II 2300 and TriStar 3020 V1.03; specific surface area and porosity), chemical analysis, thermal analysis (Netzsch STA 409 PC/PG analyzer, argon atmosphere), X-ray diffraction (XRD) (DRON-2 diffractometer; composition and structure), and scanning electron microscopy (SEM) (LEO-420 microscope). The PCA of the samples was assessed photocolorimetrically (FEK-56 PM) from the degree of decoloration of ferroin in response to illumination in the visible range and with $\lambda \geq 670$ nm light.

The Zn-modified titania samples were identified by a code, for example, 300-Zn-1, which specified the heat-treatment temperature (300°C), dopant (Zn), and nominal doping level (1 wt %). As references materials, we used undoped TiO_2 and the commercially available Degussa P25 titania.

RESULTS AND DISCUSSION

The experimental data presented in Tables 1 and 2 and Figs. 1–10 illustrate the influence of Zn content (wt %) and heat-treatment temperature (t, °C) on the structure, specific surface area (S, m^2/g), average particle size (d, nm), micropore volume (V, cm^3/g), micropore depth (h, nm), and micropore diameter (D, nm) of our samples.

The degree of zinc extraction to the X-ray amorphous material obtained by coprecipitation was found to decrease systematically with increasing added zinc content (Fig. 1). This is caused by the increased solubility of zinc hydroxide compounds in aqueous ammonia, which exceeds that in sodium hydroxide solutions. At the same time, titania is known to react with sodium hydroxide to form sodium titanates [10, 13], which we would like to avoid when preparing samples in aqueous ammonia.

After drying, the hydrolysis products had the form of X-ray amorphous powders with a specific surface area from about 200 to 430 m^2/g (5–11 nm) as determined by BET measurements. The powders contained up to 2.8 wt % NH_4^+, and 1.2 wt % Cl^-. At doping levels in the range 0.5–1 wt % Zn, the TiO_2 content of the powders was about 80 wt %, approaching that of the titanium oxyhydroxide $TiO(OH)_2$ (81.6 wt % TiO_2).

Phase formation. Raising the heat-treatment temperature of the hydrolysis products leads to a number of phase transitions (Table 1, Figs. 2–5), which depend as well on dopant concentration. At doping levels of up to 1 wt % Zn, we observe the crystallization of metastable anatase (3.52 Å) from the amorphous material starting at a temperature of 400°C and the crystallization of rutile (3.24 Å) as the temperature reaches 600°C, whereas undoped TiO_2 consists only of anatase. At doping levels of ≥5 wt % Zn, the anatase–

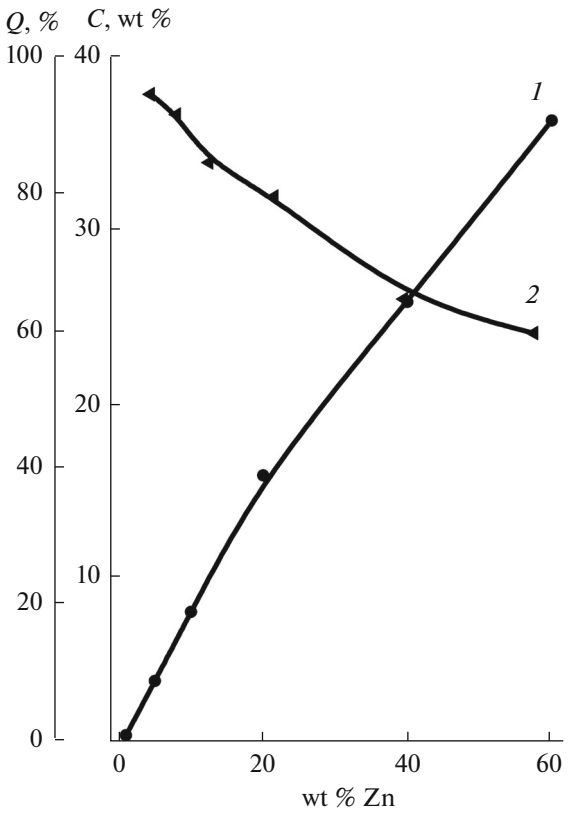

Fig. 1. (*1*) Zinc content of the synthesized materials and (*2*) degree of zinc extraction from solution as functions of added zinc content.

rutile phase transition is accompanied by the precipitation of Zn-containing phases in the form of zinc metatitanate, $ZnTiO_3$ (2.73 Å), at 800°C and zinc orthotitanate, Zn_2TiO_4 (2.54 Å), at 1150°C (Fig. 2). The phase transformations seem to occur in a wide temperature range and take a considerable time, so there are no corresponding heat effects. We believe that zinc has a promoting effect on the rutile formation process. It is worth noting that at none of the zinc concentrations used in this study was any zinc oxide phase detected. The crystallization temperature of anatase was found to increase with increasing doping level, and the temperature stability range of anatase, where no rutile was formed, was observed to decrease. In particular, at a doping level of 1 wt % Zn, anatase crystallizes at 400°C and remains stable up to a temperature of 600°C. At the same time, in the composition range 20–60 wt % Zn, there was a trace amount of anatase in an amorphous matrix at 500°C, whereas heat treatment at 600°C led to the formation of rutile and zinc titanates (Fig. 2).

Thermal analysis of the hydrolysis products also demonstrates that Zn raises the crystallization temperature of anatase (Fig. 3). With increasing Zn content, the temperature of the exothermic peak due to

Table 1. Phase composition, physicochemical properties, and PCA (E) of the synthesized materials in the Ti–O–Zn system

Sample	t, °C	Weight percent				XRD results	S, m^2/g	d, nm	E, % (for ferroin)	
		TiO_2	Cl^-	NH_4^-	Zn^{2+}		BET		visible light	$\lambda \geq 670$ nm
400-Ti	400	98.5	0.06	0.43	0	a	155	94	98	46
600-Ti	600	99.8	ND	0.02	0	a	34	45	74	21
P25	–					85% a, 15% r	48	30	49	2
20-Zn-1	20	–	–	–	–	am	207	11	–	–
80-Zn-1	80	–	–	–	–	am	429	5.3	>96	>96
300-Zn-1	300	–	–	–	–	am	266	8.6	95	92
400-Zn-1	400	–	0.1	0.38	–	a	170	5.6	60	24
500-Zn-1	500	–	–	–	–	am, a	48	32	15	9
600-Zn-1	600	99	ND	0.02	0.92	90% a, 10% r	47	32	9	2
800-Zn-1	800	–	–	–	0.95	r	1.10	1300	8.5	–
1150-Zn-1	1150	–	–	–	–	r	0.12	11900	3.5	–
20-Zn-5	20	–	–	–	–	am	242	9.5	–	–
80-Zn-5	80	–	1.2	2.78	–	am	400	5.8	>98	>96
400-Zn-5	400	–	0.1	0.44	–	am, a	217	9.2	85	72
500-Zn-5	500	–	–	–		a	20.2	76	35	24
600-Zn-5	600	97	ND	0.01	3.9	82% a, 18% r	19.6	78	21	10
800-Zn-5	800	–	–	ND	4.1	r, $ZnTiO_3$	1.18	1210	12	0
900-Zn-5	900	–	–	–	–	r, $ZnTiO_3$	–	–	–	–
1150-Zn-5	1150	–	–	–	–	r, Zn_2TiO_4	0.17	8240	7.6	0
20-Zn-10	20	–	–	–	–	am	219	10	–	–
80-Zn-10	80	–	1.0	2.64	–	am	420	5.5	>96	>96
300-Zn-10	300	–	–	–	–	am	278	8.3	93	92
400-Zn-10	400	–	0.1	0.35	–	am, a	271	7.4	77	74
500-Zn-10	500	–	–	–	–	a	89	17	35	24
600-Zn-10	600	95	ND	0.01	8.0	a, r, $ZnTiO_3$	18.6	62	27	16
800-Zn-10	800	–	–	–	–	r, $ZnTiO_3$	1.3	1090	15	–
1150-Zn-10	1150	–	–	–	–	r, Zn_2TiO_4	0.18	7650	7.1	–
20-Zn-20	20	–	–	–	–	am	232	9.9	–	–
80-Zn-20	80	–	0.91	2.44	–	am	307	7.5	>96	>96
400-Zn-20	400	–	0.2	0.37	–	am	233	9.9	93	90
500-Zn-20	500	–	–	–	–	am, a	91	22	50	39
600-Zn-20	600	90	ND	0.01	16.1	a, r, $ZnTiO_3$	18	77	30	15
800-Zn-20	800	–	–	–		r, $ZnTiO_3$	1.26	1064	25	–
1150-Zn-20	1150	–	–	–	–	r, Zn_2TiO_4	0.16	8360	7.1	–
80-Zn-40	80	–	1.2	2.8	–	am	382	6.0	>96	60
400-Zn-40	400	–	0.1	0.35	–	am	267	8.6	94	68
500-Zn-40	500	–	–	–	24	am, a	166	12	60	54

Table 1. (Contd.)

Sample	t, °C	Weight percent				XRD results	S, m^2/g	d, nm	E, % (for ferroin)	
		TiO_2	Cl^-	NH_4^-	Zn^{2+}		BET		visible light	$\lambda \geq 670$ nm
600-Zn-40	600	82	ND	0.01	–	a, r, $ZnTiO_3$	37	39	24	17
800-Zn-40	800	–	–	–		r, $ZnTiO_3$	1.15	1240	8.5	0
1150-Zn-40	1150	–	–	–	–	r, Zn_2TiO_4	0.11	12990	5.3	0
80-Zn-60	80	–	1.2	2.78	–	am	268	8.6	>96	65
400-Zn-60	400	–	0.1	0.39	–	am	137	17	81	70
500-Zn-60	500	–	–		36.7	am, a (tr)	89	23	60	55
600-Zn-60	600	70	ND	0.01	–	a, r, $ZnTiO_3$	56	27	21	18
800-Zn-60	800	–	–	–	36.5	r, $ZnTiO_3$	1.16	1230	8.5	0
850-Zn-60	850	–	–	–	–	r, $ZnTiO_3$, Zn_2TiO_4, $Zn_2Ti_3O_8$	–	–	–	–
950-Zn-60	950	–	–	–	–	r, $ZnTiO_3$, Zn_2TiO_4	–	–	–	–
1150-Zn-60	1150	–	–	–	–	r, Zn_2TiO_4	0.04	35710	3.5	0

am = amorphous phase, a = anatase, r = rutile, ND = not detected; the symbol – denotes that no determination was made.

Table 2. Influence of zinc content and heat-treatment temperature on the texture characteristics of the Zn-modified TiO_2 samples

t, °C	V, cm^3/g	h, nm	D, nm	t, °C	V, cm^3/g	h, nm	D, nm
Zn-1				**Zn-5**			
20	0.16	3.69	3.86	20	0.16	3.24	4.07
80	0.31	3.34	3.54	80	0.33	3.76	4.30
300	–	–	–	300	0.34	5.08	4.56
400	0.31	7.23	5.52	400	0.35	6.16	5.12
500	0.15	8.93	6.72	500	0.06	11.95	9.27
600	0.15	11.93	9.10	600	0.08	15.76	12.81
800	0.02	16.28	42.4	800	0.02	14.54	40.99
Zn-10				**Zn-20**			
20	0.17	3.64	4.48	20	0.10	2.49	3.24
80	0.34	3.70	4.61	80	0.15	2.60	3.02
300	0.37	5.30	5.02	300	0.24	3.94	4.04
400	0.38	5.49	5.07	400	0.22	3.79	3.72
500	0.25	10.37	8.33	500	0.18	7.67	5.98
600	0.082	16.41	12.73	600	0.09	17.55	15.72
800	0.016	14.32	44.16	800	–	–	–
Zn-40				**Zn-60**			
80	0.48	4.88	5.99	80	0.45	6.17	7.56
300	0.49	5.95	5.99	300	0.35	7.04	7.57
400	0.45	6.94	8.37	400	0.32	8.80	8.29
500	0.40	9.22	7.78	500	0.30	12.05	10.57
600	0.27	24.15	23.77	600	0.25	16.08	14.76

V, h, and D are the pore volume, depth, and diameter, respectively.

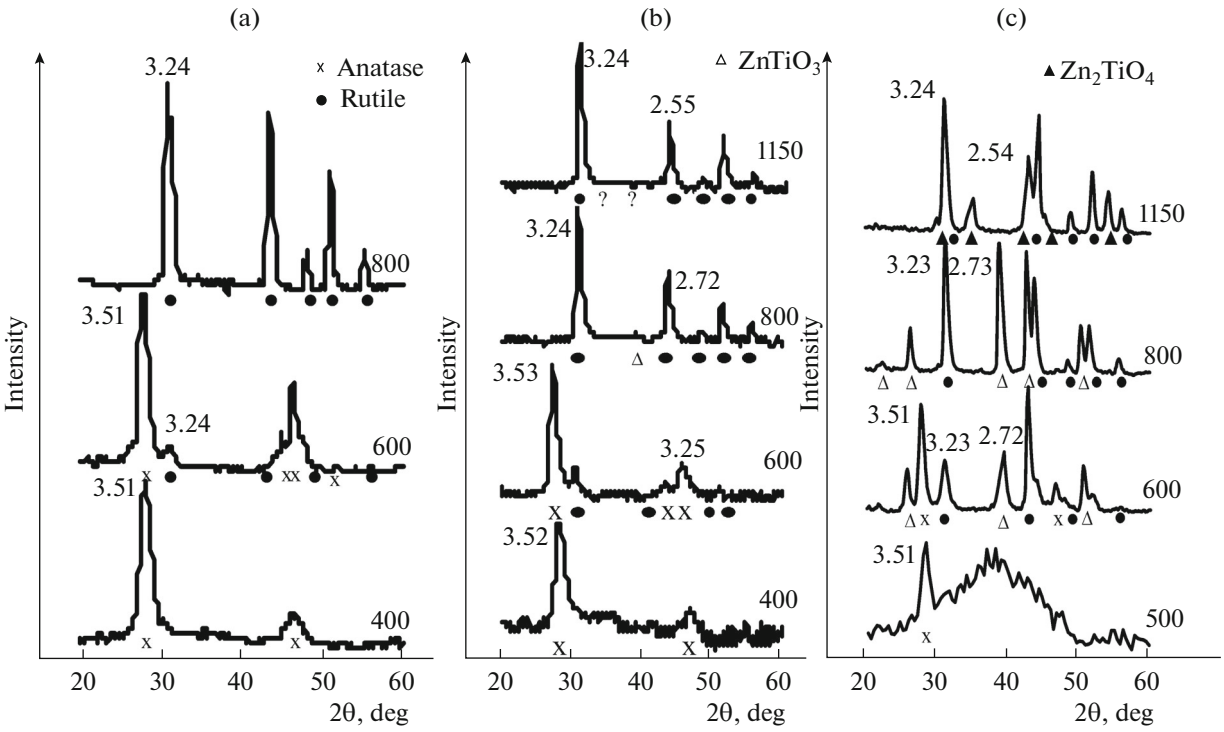

Fig. 2. X-ray diffraction patterns of Zn-modified titania obtained at various heat-treatment temperatures (numbers at the scans, degrees Celsius) and Zn doping levels: (a) 1, (b) 5, and (c) 60 wt % Zn.

anatase crystallization increases from 412.2°C for undoped titania to 496.2°C at 60 wt % Zn.

DSC curves of the Zn-modified materials are similar to that of TiO_2, suggesting that the $TiCl_4$–$ZnCl_2$ cohydrolysis products have a hydroxide nature. The only endothermic peak in all of the DSC curves (Fig. 3), in combination with the shape of the weight loss (TG) curves, indicates that the dehydration process and the removal of volatile components occur in one step and reach completion at temperatures near 400°C. The decrease in the temperature of the endothermic peak with increasing zinc concentration, from 145.8°C for undoped titania to 124.9°C for the Zn-60 samples, suggests that the incorporation of zinc into the composition of the hydrolysis products facilitates the dehydration process. Chemical analysis data indicate that this is accompanied by the removal of volatile species from the hydrolysis products: chloride ions and ammonia groups (Table 1).

Thus, the synthesis products in the Ti–O–Zn system undergo the following sequence of phase transitions: X-ray amorphous phase → anatase (TiO_2) → rutile (TiO_2) and/or $ZnTiO_3$, Zn_2TiO_4, and $Zn_2Ti_3O_8$. Another characteristic feature of this system is the formation of about nine mixed-phase regions (Fig. 4). Zinc precipitates first as zinc metatitanate, $ZnTiO_3$ (hexagonal structure), and then as zinc orthotitanate, Zn_2TiO_4 (cubic structure), at temperatures above 900°C. In the samples containing 60 wt % Zn (850-Zn-60 and 900-Zn-60), one more oxide phase crystallizes in this temperature range: $Zn_2Ti_3O_8$ with a cubic structure (2.54, 5.85, 5.90 Å). The Ti–O–Zn system undergoes many structural changes. Together with changes in particle size, this would be expected to influence the photocatalytic properties of the materials.

Morphology. Raising the heat-treatment temperature of the hydrolysis products first leads to an increase in their specific surface area (for example, from 207 to 429 m^2/g in Zn-1) due to the loosening caused by the dehydration process and the removal of volatile components from the precipitates. This step is followed by a reduction in the specific surface area of the powders, which is particularly accelerated by the crystallization of anatase, rutile, and zinc titanates of various compositions, as well as by the aggregation and agglomeration of crystallites (Table 1, Fig. 5). The structural changes that take place as the heat-treatment temperature of the hydrolysis products is raised are also responsible for the changes in the particle size of the Zn-modified titania samples. The specific surface area of the X-ray amorphous synthesis products varies from 180 to 430 m^2/g (crystallite size from 5 to 13 nm), depending on Zn content and heat-treatment temperature. The specific surface area of anatase ranges from 160 to 200 m^2/g (6–11 nm). That of mixed phases (anatase, rutile, zinc metatitanate, and zinc orthotitanate) is smaller, 36–70 m^2/g (40–57 nm), and heat treatment at 1150°C reduces it to below

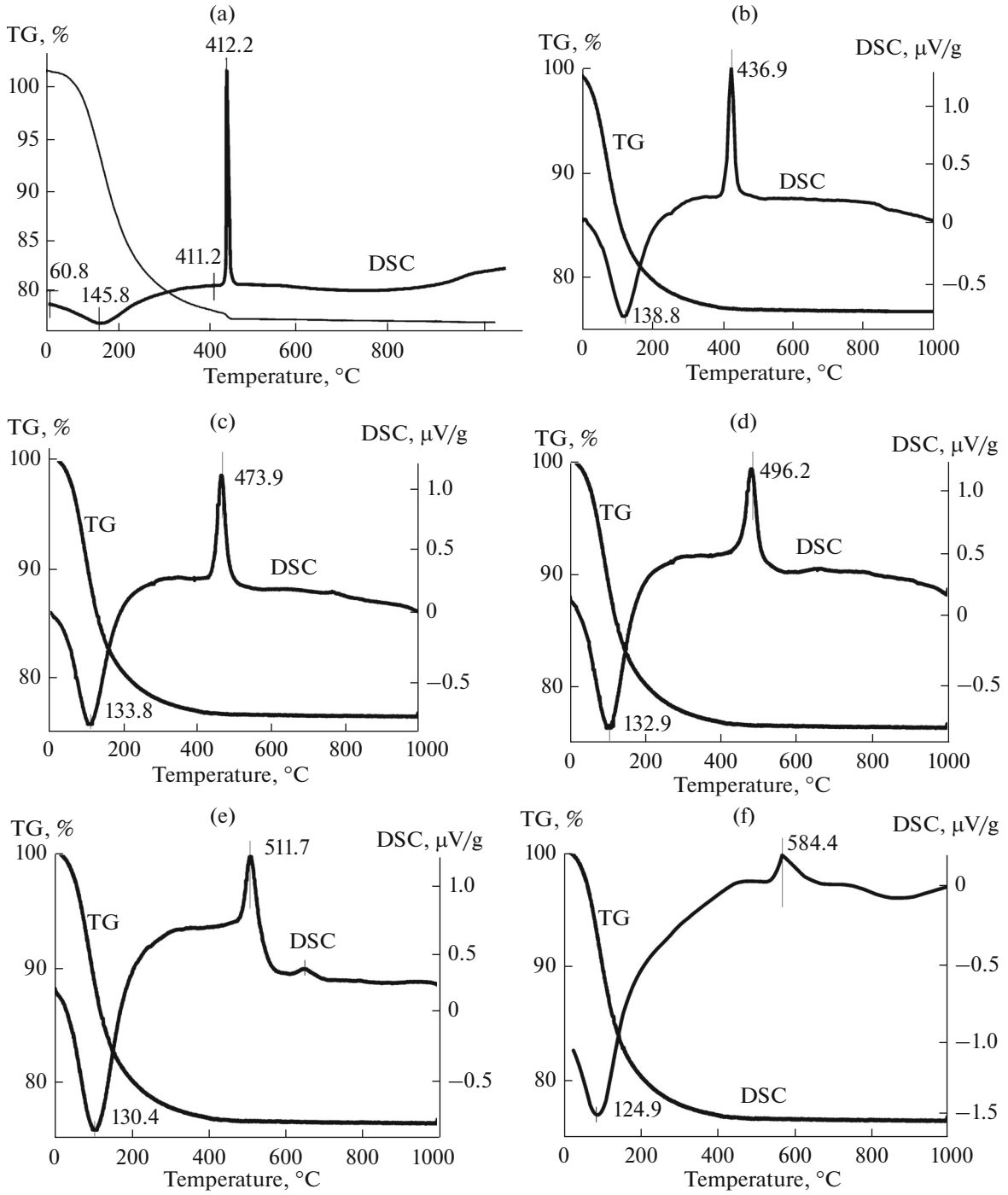

Fig. 3. Thermal analysis data for Zn-modified TiO_2: (a) 0, (b) 1, (c) 5, (d) 10, (e) 20, and (f) 60 wt % Zn.

0.1 m^2/g (13 μm). Thus, both the X-ray amorphous powders and the multiphase samples before heat treatment in the range 800–900°C have a large specific surface area and consist of nanoparticles (Table 1). The powders calcined at higher temperatures are subject to agglomeration processes and consist of micron-sized particles (Table 1, Fig. 7).

The plot of micropore volume (V) versus heat-treatment temperature has a maximum, with the largest micropore volume (0.3–0.5 cm^3/g) at heat-treatment temperatures from 200 to 400°C, which is probably the consequence of the rapid water removal from the oxyhydroxide hydrolysis products (Table 2, Fig. 6).

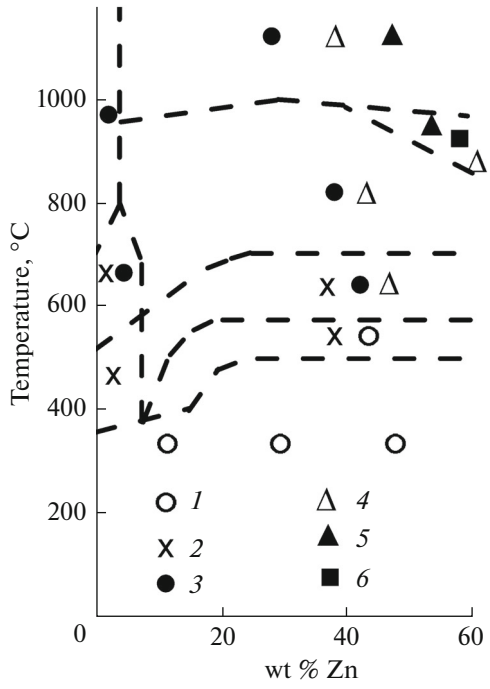

Fig. 4. Influence of Zn content and heat-treatment temperature on the phase composition of the synthesized materials: (*1*) X-ray amorphous phase, (*2*) anatase, (*3*) rutile, (*4*) $ZnTiO_3$, (*5*) Zn_2TiO_4, (*6*) $Zn_2Ti_3O_8$.

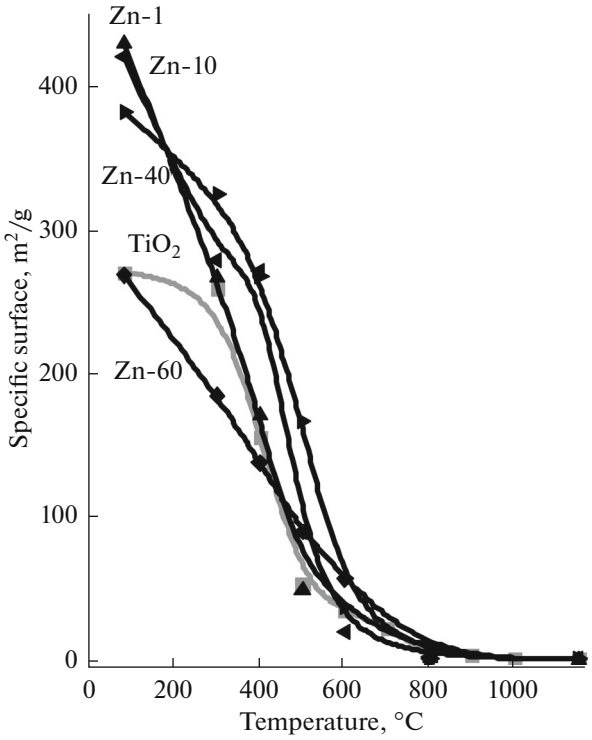

Fig. 5. Specific surface area as a function of heat-treatment temperature and zinc content for the synthesized materials.

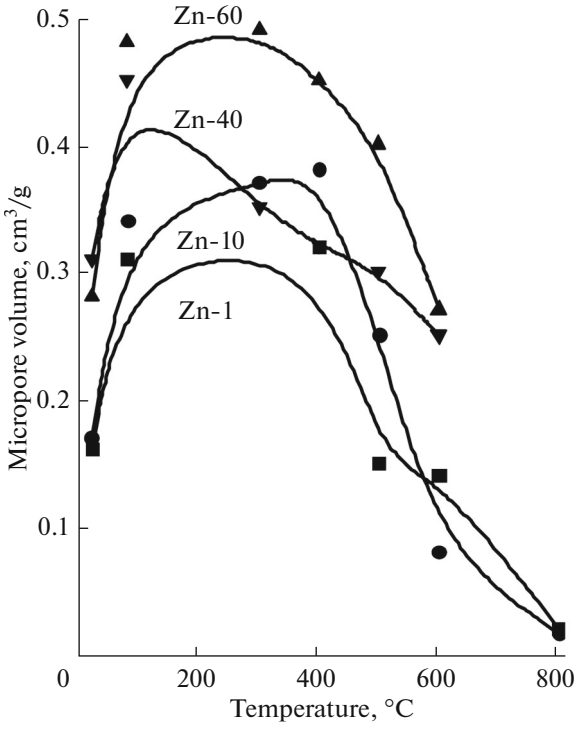

Fig. 6. Micropore volume as a function of heat-treatment temperature and Zn content for the synthesized materials.

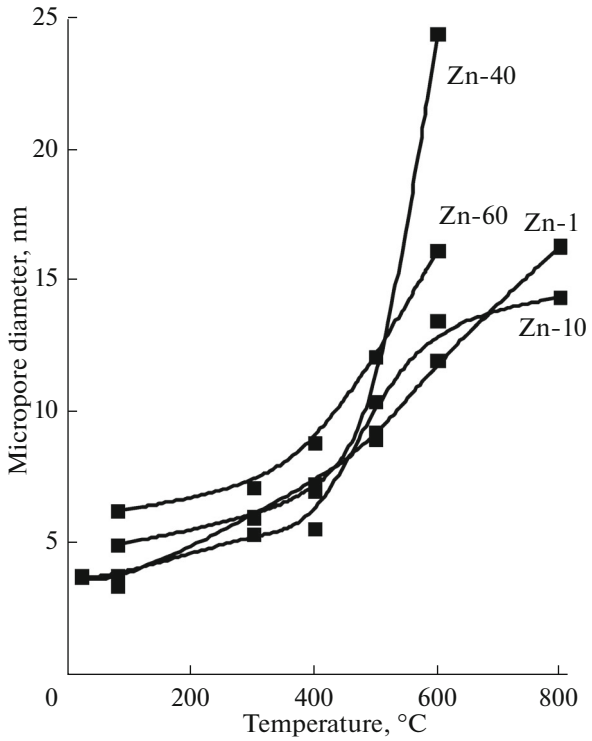

Fig. 7. Micropore diameter as a function of heat-treatment temperature and Zn content for the synthesized materials.

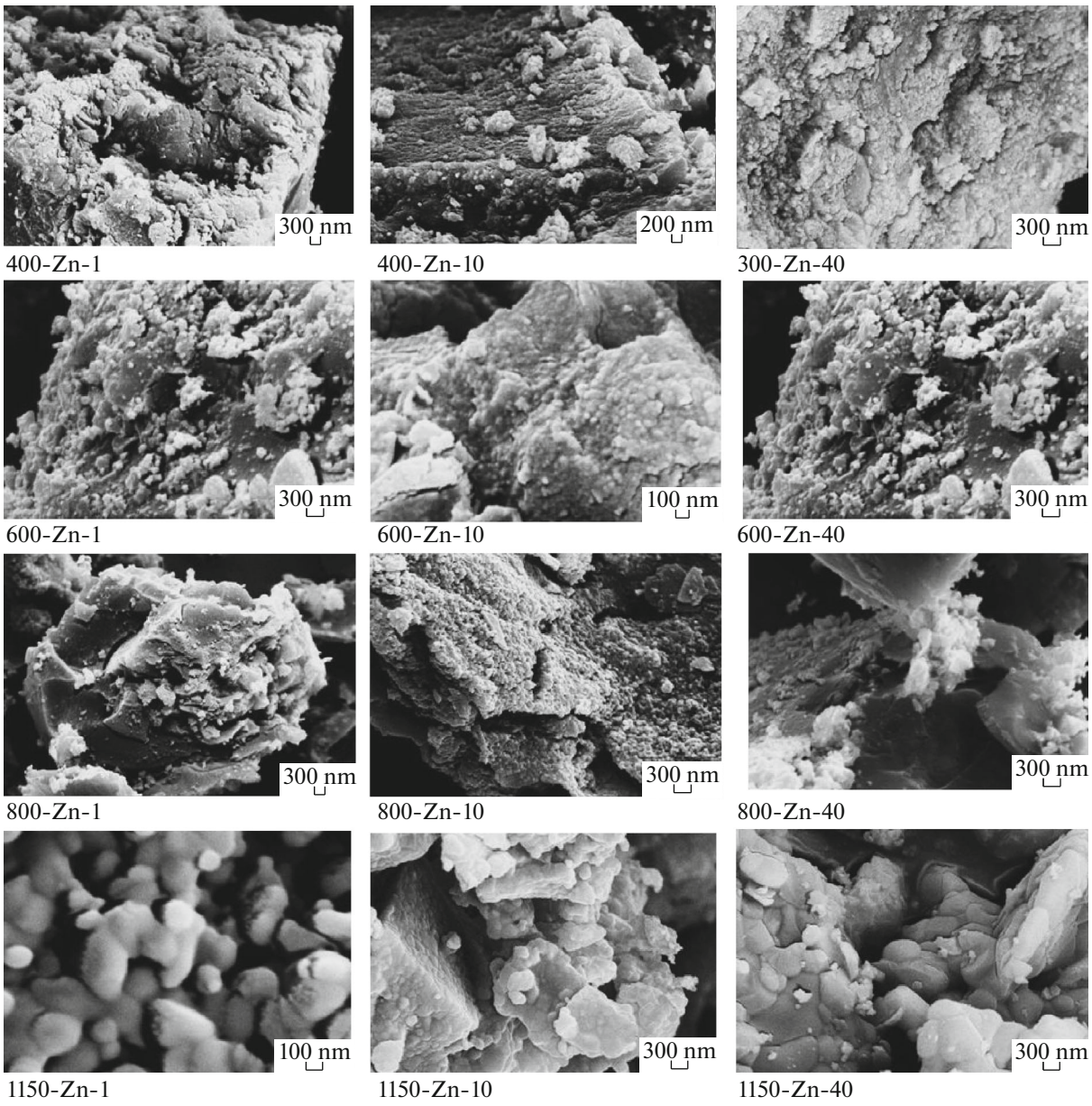

Fig. 8. SEM micrographs of the surface of particles in the materials synthesized at temperatures from 300 to 1150°C (see Fig. 4 for phase compositions).

The micropore depth in the samples is comparable to the micropore diameter: for example, 3.34 and 3.54 nm in the 80-Zn-1 sample, 5.49 and 5.07 nm in 400-Zn-10, and 24.15 and 23.77 nm in 600-Zn-40, respectively. Both the micropore depth h and micropore diameter D (Fig. 7) increase with increasing heat-treatment temperature.

The SEM micrographs in Fig. 8 demonstrate that the Zn-containing materials prepared at heat-treatment temperatures from 300 to 1150°C are polydisperse. The X-ray amorphous materials consist of large, irregularly shaped aggregates of nanoparticles. With increasing heat-treatment temperature, the particle size increases in all of the samples to give separate rounded, monomorphic crystallites, which is best illustrated by the example of the 1150-Zn-1 sample. The particles sinter to form bulk aggregates up to tens of microns in size, having bumps on smooth surfaces.

Photocatalytic activity. The PCA of the Zn-modified titania samples for ferroin degradation reaction is a rather strong and intricate function of the doping level, heat-treatment temperature, and phase composition (Table 1, Figs. 9, 10).

At a given heat-treatment temperature, the PCA of the samples increases with increasing Zn content,

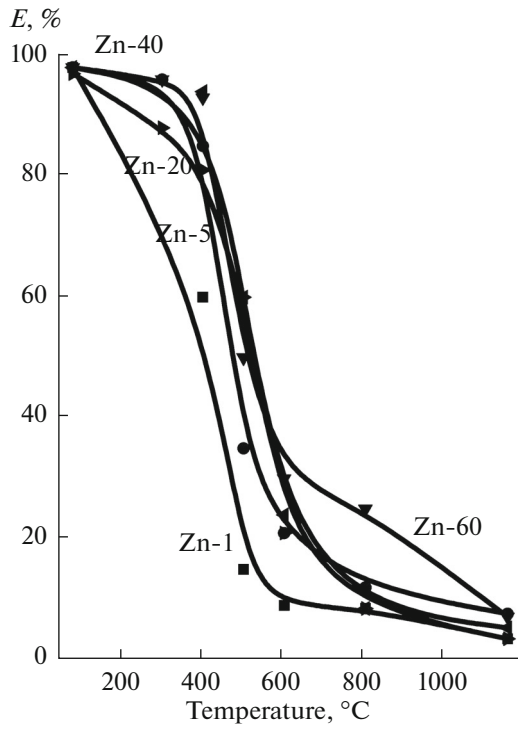

Fig. 9. PCA as a function of heat-treatment temperature and Zn content for the synthesized materials.

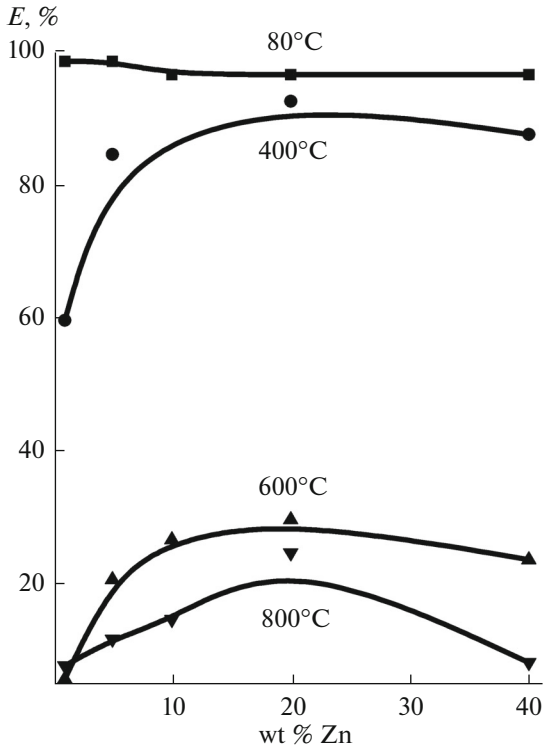

Fig. 10. PCA as a function of Zn content and heat-treatment temperature for the synthesized materials.

whereas their specific surface area decreases (Figs. 5, 9). The highest PCA is offered by the X-ray amorphous and poorly crystallized samples, which have the largest specific surface area (Fig. 10).

The appreciable PCA of the Zn-rich samples calcined at temperatures from 500 to 600°C has important implications for possible photocatalyst regeneration and high-temperature photocatalysis.

Thus, the present results demonstrate that a number of Zn-modified titania materials exhibit higher PCA under illumination with visible light than does undoped TiO_2 of a similar origin and the commercially available Degussa P25 photocatalyst, which is evidence of their significant spectral sensitization (Table 1).

CONCLUSIONS

We have synthesized materials based on titanium(IV) and zinc(II) oxides, containing 1 to 60 wt % Zn, with the formation of multiphase compositions (X-ray amorphous phase and/or anatase, rutile, $ZnTiO_3$, and Zn_2TiO_4) and studied their phase transitions, morphology, and PCA. Increasing the Zn content of the materials is favorable for their spectral sensitization, including the range $\lambda \geq 670$ nm.

The highest PCA under illumination with visible light, exceeding that of the commercially available Degussa P25 titania is offered by the nanomaterials having a specific surface area above 50 m^2/g and containing 10–30 wt % Zn.

ACKNOWLEDGMENTS

This work was supported by the Russian Federation Ministry of Education and Science, grant no. NSh 487.2014.3.

REFERENCES

1. Ding Xing, Ai Zhihui, and Zhang Lizhi, Design of a visible light driven photo-electrochemical/electro-Fenton coupling oxidation system for wastewater treatment, *J. Hazardous Mater.,* 2012, vols. 239–240, pp. 233–240.
2. Kanakkanmavudi, J.B., Baiju, K.V., Swapankumar, G., and Warrier, K.G.K., A novel approach for enhanced visible light activity in doped nanosize titanium dioxide through the excitons trapping, *J. Solid State Chem.,* 2012, vol. 186, pp. 149–157.
3. Gavrilov, A.I., Rodionov, I.A., Gavrilova, D.Yu., Zvereva, I.A., Churagulov, B.R., and Tret'yakov, Yu.D., Hydrothermal route to titania-based nanoparticles for photocatalytic water splitting, *Dokl. Chem.,* 2012, vol. 444, no. 2, pp. 133–136.
4. Sedneva, T.A., Lokshin, E.P., Belikov, M.L., and Kalinnikov, V.T., Photocatalytic activity of tungsten-modified titanium oxide, *Dokl. Phys. Chem.,* 2012, vol. 443, no. 1, pp. 57–59.

5. Sedneva, T.A., Lokshin, E.P., Belikov, M.L., and Belyaevskii, A.T., TiO_2- and Nb_2O_5-based photocatalytic composites, *Inorg. Mater.,* 2013, vol. 49, no. 4, pp. 382–389.

6. Gavrilov, A.I., Kapitanova, O.O., Baranov, A.N., and Churagulov, B.R., Specifics of hydrothermal synthesis of oriented zinc oxide nanorods on metallic zinc substrates, *Russ. J. Inorg. Chem.,* 2012, vol. 57, no. 9, pp. 1182–1186.

7. Lebedev, V.A., Gavrilov, A.I., Shaporev, A.S., Ivanov, V.K., Churagulov, B.R., and Tret'yakov, Yu.D., Hydrothermal and hydrothermal–microwave synthesis of oriented nanorods of zinc oxide on an ITO substrate, *Dokl. Chem.,* 2012, vol. 444, no. 1, pp. 117–119.

8. Benehkohal, N.P. and Demopoulos, G.P., Green preparation of TiO_2–ZnO nanocomposite photoanodes by aqueous electrophoretic deposition, *J. Electrochem. Soc.,* 2012, vol. 159, no. 5, pp. 602–610.

9. Gavrilov, A.I., Baranov, A.N., Churagulov, B.R., and Mikhailov, B.P., Hydrothermal synthesis of aligned zinc oxide nanorod arrays on aluminum- and antimony-doped metallic zinc substrates, *Nanosistemy,* 2012, vol. 3, no. 2, pp. 90–99.

10. Gavrilov, A.I., Balakhonov, C.V., Gavrilova, D.Yu., Churagulov, B.R., and Gudilin, E.A., Hydrothermal synthesis of sodium and potassium titanates and their photocatalytic properties in water and methanol/water splitting, *Dokl. Chem.,* 2014, vol. 455, nos. 1–2, pp. 58–61.

11. Surkin, R.R., Zhimalov, A.B., Bondareva, L.N., Gorina, I.N., Gerancheva, O.E., and Polkan, G.A., RF Patent 2 434 819, *Byull. Izobret.,* 2011, no. 33.

12. Kushnir, S.E., Gavrilov, A.I., Grigor'eva, A.V., Trusov, L.A., Churagulov, B.R., Kazin, P.E., and Tret'yakov, Yu.D., Single-step hydrothermal synthesis of single-domain strontium hexaferrite particles, *Al'tern. Energ. Ekol.,* 2010, no. 8, pp. 84–87.

13. Sedneva, T.A., Lokshin, E.P., Belikov, M.L., and Belyaevskii, A.T., Preparation and properties of photocatalytic composites based on titanium(IV), copper(II), and sodium(I) oxides, *Inorg. Mater.,* 2014, vol. 50, no. 11, pp. 1104–1113.

Translated by O. Tsarev